Application of the Adaptive Mesh Refinement Technique to Particle-in-Cell Simulations of Beams and Plasmas*

J-L Vay, C. G. R. Geddes - Lawrence Berkeley National Laboratory
D. P. Grote, A. Friedman, S. M. Lund - Lawrence Livermore National Laboratory

The development of advanced accelerators often requires the modeling of systems that involve a wide range of scales in space and/or time, which can render such modeling extremely challenging. The Adaptive Mesh Refinement technique can be used to significantly reduce the requirements for computer memory and the number of operations. Its application to the fully self-consistent modeling of beams and plasmas is especially challenging, due to properties of the Vlasov-Maxwell system of equations. Most recently, we have begun to explore the application of AMR to the modeling of laser plasma wakefield accelerators (LWFA). We present a summary of the main issues and their mitigations, as well as examples of applications.

*Supported by the US-DOE under Contracts DE-AC02-05CH11231 and DE-AC52-07NA27344, and a US-DOD SPIB phase II. Used resources of NERSC, supported by the US-DOE under Contract DE-AC02-05CH11231.

Combining Adaptive Mesh Refinement with Particle-In-Cell techniques: the difficulties

Mesh refinement implies a jump of resolution from which may result:
- loss of symmetry: self-force[1,2],
- loss of conservation laws[1,2],
- EM: waves reflection[3].

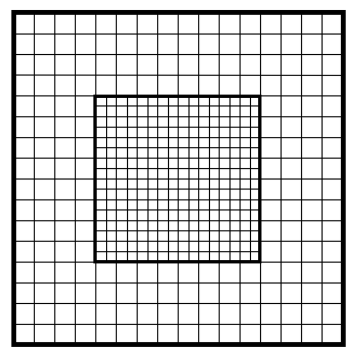

(1) Vay et al., *Laser Part. Beams* 20 (2002)
(2) Vay et al., *Phys. Plasmas* 11 (2004)
(3) Vay, *J. Comput. Phys.* 167 (2001)

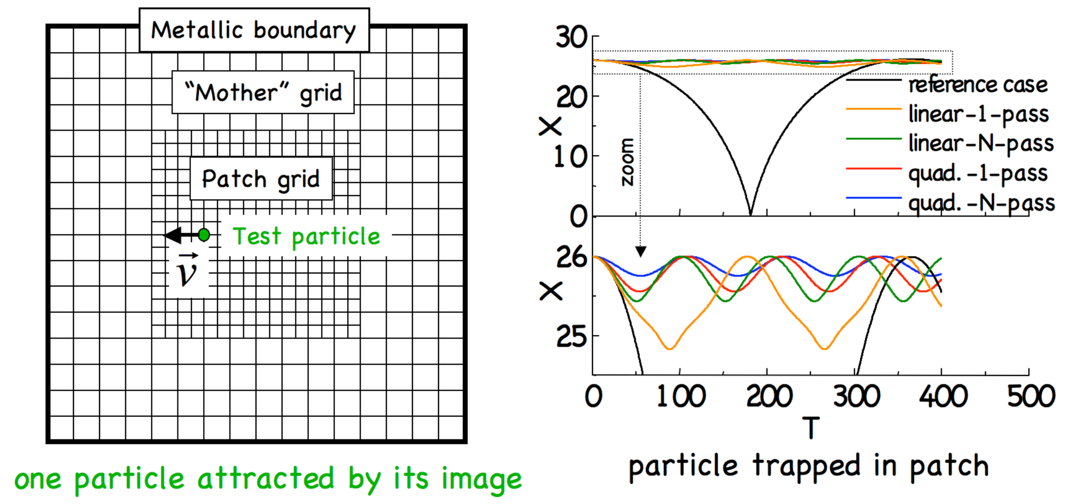

*J.-L. Vay et al., *Laser Part. Beams* **20**, 569 (2002)

⇒ MR introduces spurious force,

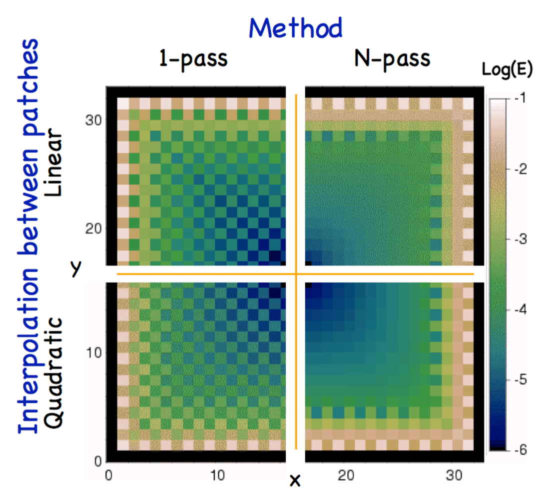

Magnitude of spurious force decreases rapidly with distance to edge of patch.

The spurious force effect is revealed for example in 2-D simulations* of the time evolution of one charged particle interacting with its electrostatic image force generated by a nearby perfect conductor (specular reflection is applied on the particle motion when it hits the wall). When a refinement patch involving interpolation at the interface is introduced, a spurious force prevents the particle from leaving the patch.

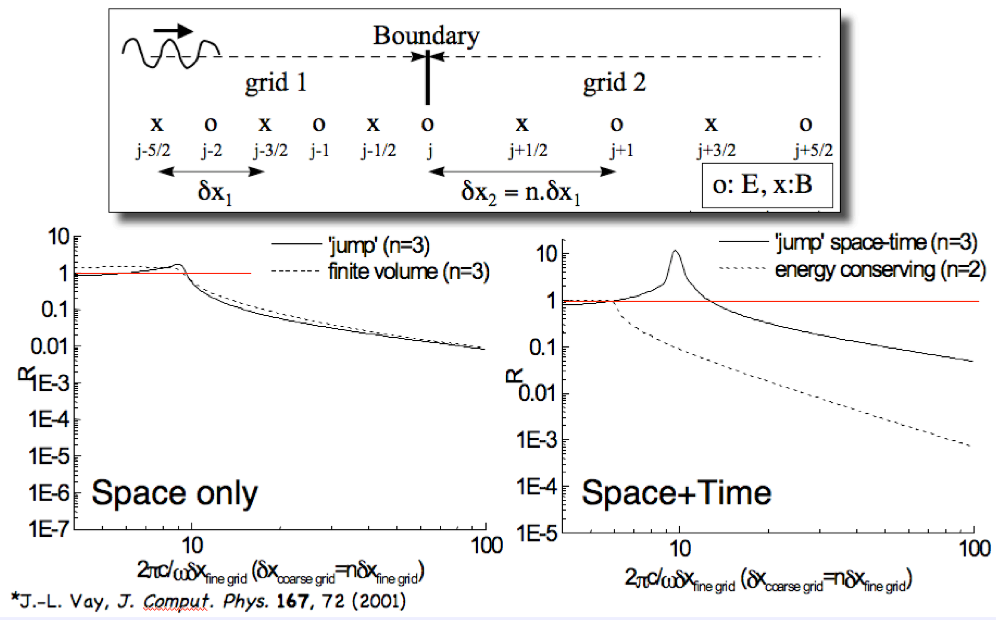

*J.-L. Vay, *J. Comput. Phys.* **167**, 72 (2001)

Spurious reflection of electromagnetic waves are revealed in 1-D simulations* of a sinusoidal wave crossing a fine-to-coarse boundary, using various interpolation schemes.

Combining Adaptive Mesh Refinement with Particle-In-Cell techniques: our solutions

Electrostatics[1,2]

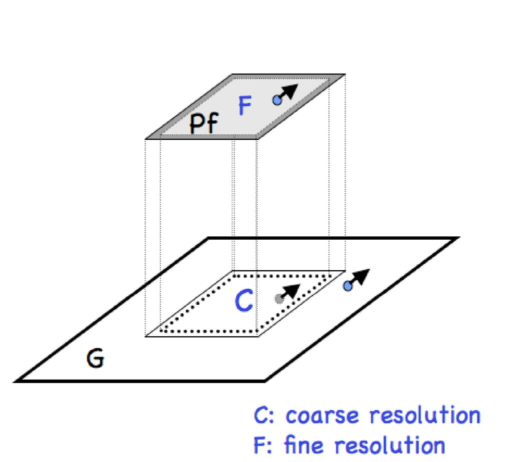

User controls relative magnitude of spurious force[2].

(1) Vay et al., *Laser Part. Beams* **20** (2002)
(2) Vay et al., *Phys. Plasmas* **11** (2004)

Electromagnetic[3]

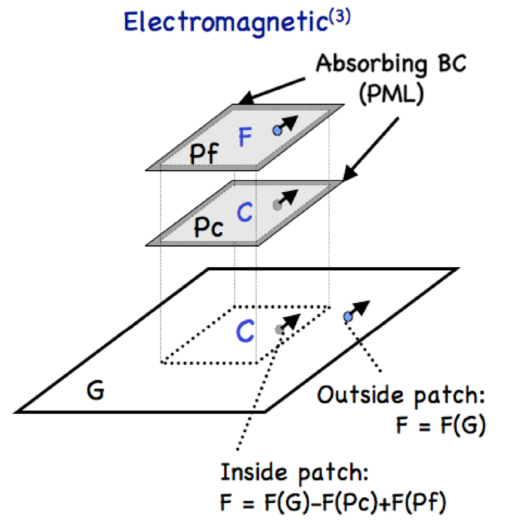

User controls relative magnitude of spurious force & wave reflections.

(3) Vay, Adam, Heron, *Comp. Phys. Comm.* **164** (2004)

Our methods rely on the separation of the calculation in the parent grids and their refinement patches (i.e. patches are not embedded in parent grids and there is no interpolation at interfaces), and on buffer regions to control spurious effects.

The Maxwell equations were modified* to allow for iterative removal of spurious charges at the PML interface.

$$\frac{\partial\vec{B}}{\partial t} = -\vec{\nabla}\times\vec{E}$$
$$\frac{\partial\vec{E}}{\partial t} = \vec{\nabla}\times\vec{B} - \vec{J} + \vec{\nabla}F$$
$$\frac{\partial F}{\partial t} = \vec{\nabla}\cdot\vec{E} - \rho$$

* J.-L. Vay & C. Deutsch, *Fus. Eng. & Design* 32-33, 467 (1996)

Due to discretization, the standard Yee solver leads to different wave dispersions in vacuum in grids of different resolutions. This may cause spurious effects with the mesh refinement scheme. In order to circumvent this issue, we have adapted the stencil from Karkkainen*, which offers better dispersion than the Yee scheme. We showed that for full benefit, at Δt=cΔx, a binomial filter must be applied to the source terms, in order to remove spurious oscillations at the Nyquist frequency that may cause an instability.

Enlarged stencil* => no disp. in x,y,z

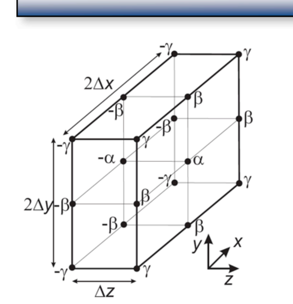

$$E_x|^{n+1}_{i+1/2,j,k} = E_x|^{n}_{i+1/2,j,k} - \alpha\frac{\Delta t}{\epsilon_0}D_{z,0}H_y|^{n+1/2}_{i+1/2,j,k} - 4\beta\frac{\Delta t}{\epsilon_0}D_{z,1}H_y|_{i+1/2,j,k} - 4\gamma\frac{\Delta t}{\epsilon_0}D_{z,2}H_y|^{n+1/2}_{i+1/2,j,k} + \alpha\frac{\Delta t}{\epsilon_0}D_{y,0}H_z|^{n+1/2}_{i+1/2,j,k} + 4\beta\frac{\Delta t}{\epsilon_0}D_{y,1}H_z|^{n+1/2}_{i+1/2,j,k} + 4\gamma\frac{\Delta t}{\epsilon_0}D_{y,2}H_z|^{n+1/2}_{i+1/2,j,k}.$$

Stencil on H unchanged

Implementation in Warp

$$H_x|^{n+1}_{i+1/2,j,k} = H_x|^{n}_{i+1/2,j,k} - \alpha\frac{\Delta t}{\epsilon_0}D_{z,0}E_y|^{n+1/2}_{i+1/2,j,k} - 4\beta\frac{\Delta t}{\epsilon_0}D_{z,1}E_y|_{i+1/2,j,k} - 4\gamma\frac{\Delta t}{\epsilon_0}D_{z,2}E_y|^{n+1/2}_{i+1/2,j,k} + \alpha\frac{\Delta t}{\epsilon_0}D_{y,0}E_z|^{n+1/2}_{i+1/2,j,k} + 4\beta\frac{\Delta t}{\epsilon_0}D_{y,1}E_z|^{n+1/2}_{i+1/2,j,k} + 4\gamma\frac{\Delta t}{\epsilon_0}D_{y,2}E_z|^{n+1/2}_{i+1/2,j,k}.$$

- E and H switched,
  => E push same as Yee,
- exact charge conservation preserved in 2D & 3D with unmodified Esirkepov current deposition and implied enlarged stencil on div E.

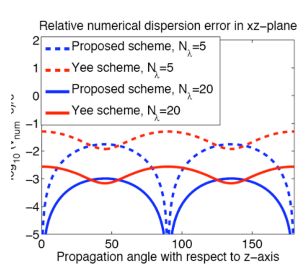

Issues for PIC:

- source terms are not given,
- odd-even oscillation when Δt=Δx/c.

1-2-1 filter needed at Δt=Δx/c

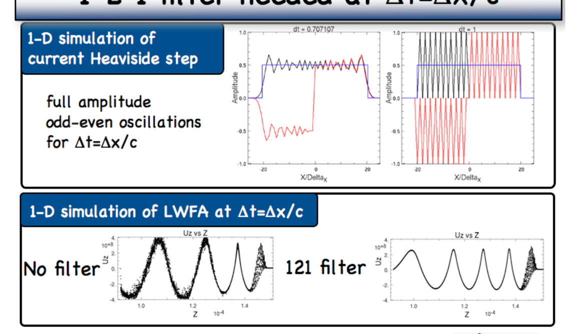

*M. Karkkainen, et al., Proceedings of ICAP 2006, Chamonix, France

The Warp package

Warp combines features of plasma and accelerator simulation codes

- **Geometry:** 3-D (x,y,z), 2-D (x,y), (x,z) or axisym. (r,z)
- **Field solvers:** ES - FFT, multigrid, AMR; implicit
  EM - Yee mesh, PML, AMR
- **Particle movers:** Boris, large time step "drift-Lorentz", new relativistic Leapfrog
- **Boundaries:** "cut-cell" --- no restriction to "Legos"
- **Lattice:** general; non-paraxial; can read MAD files
  - solenoids, dipoles, quads, sextupoles, linear maps, arbitrary fields, acceleration
- **Bends:** "warped" coordinates; no "reference orbit"
- **Reference frame:** lab, moving-window, boosted
- **Diagnostics:** extensive snapshots and histories
- **Parallel:** MPI (1, 2 and 3-D domain decomposition)
- **Python and Fortran:** "steerable," input decks are programs
- **Misc.:** **trajectory** tracing, quasistatic & steady-flow modes, space charge emitted emission, models for electron-cloud and gas effects

Quasi-linear speedup on strong scaling test on Franklin

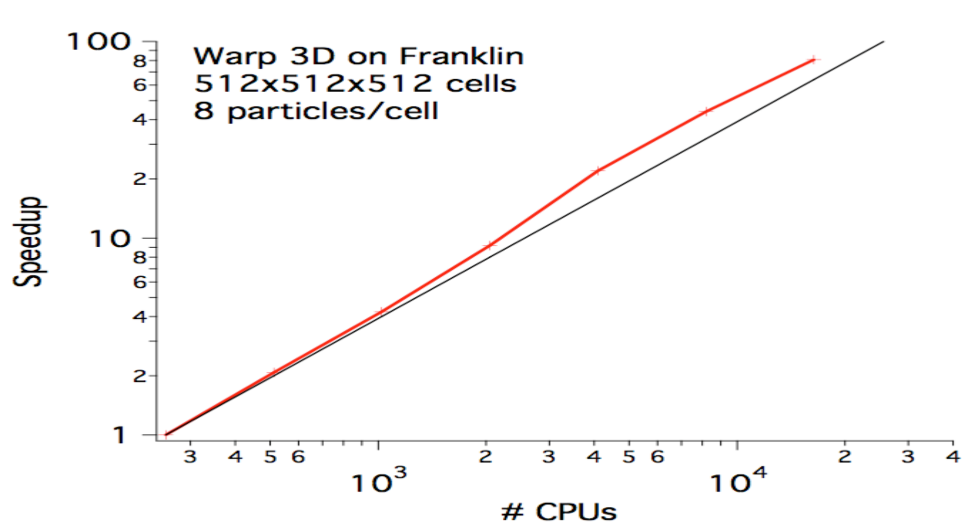

Example of electrostatic AMR PIC simulations

2-D axisymmetric simulations have shown that a high resolution is needed to capture the details that are necessary for accurate modeling of a Heavy Ion Fusion ion beam source. Speedup of ~10 was obtained with the use of AMR.

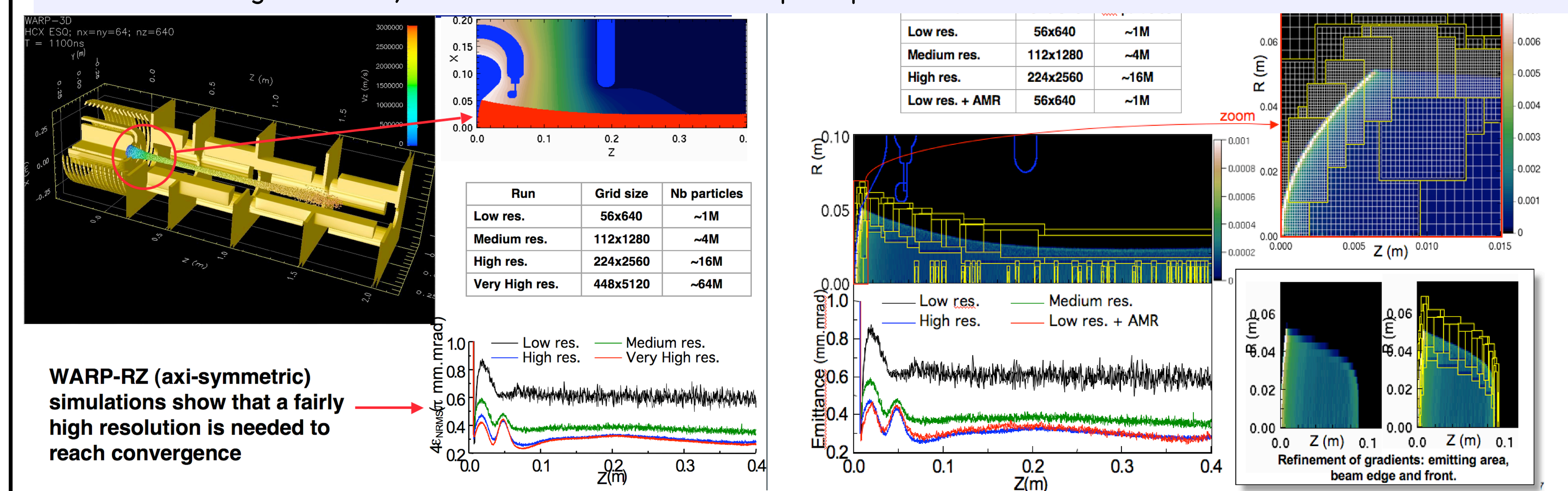

Run	Grid size	Nb particles
Low res.	56x640	~1M
Medium res.	112x1280	~4M
High res.	224x2560	~16M
Very High res.	448x5120	~64M

Low res.	56x640	~1M
Medium res.	112x1280	~4M
High res.	224x2560	~16M
Low res. + AMR	56x640	~1M

Examples of electromagnetic MR simulations

High resolution is needed for accurate simulation of plasma wakes generated by a hard-edged, elliptical, "frozen" (rigid) beam propagating at constant velocity $v_z = 0.5c$ through an initially cold neutral plasma of initial density n_0. 2-1/2D (below) and 3D (right) Warp simulations showed that the computation cost could be greatly reduced by using 2 levels of mesh refinement, and adjusting the number and weights of injected plasma macroparticles.

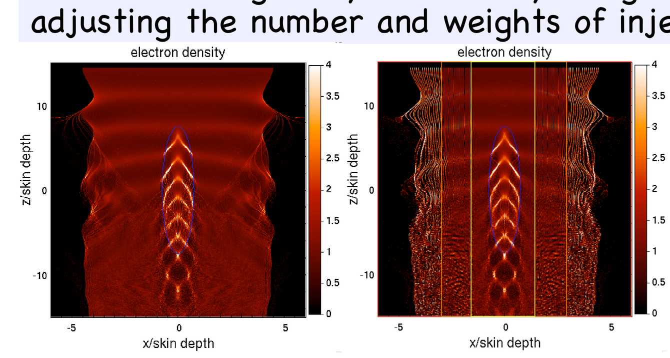

A run was performed with no plasma injected in the coarse grids, to confirm their importance for accuracy.

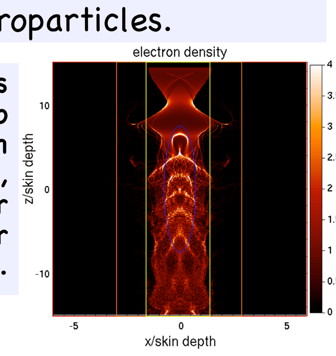

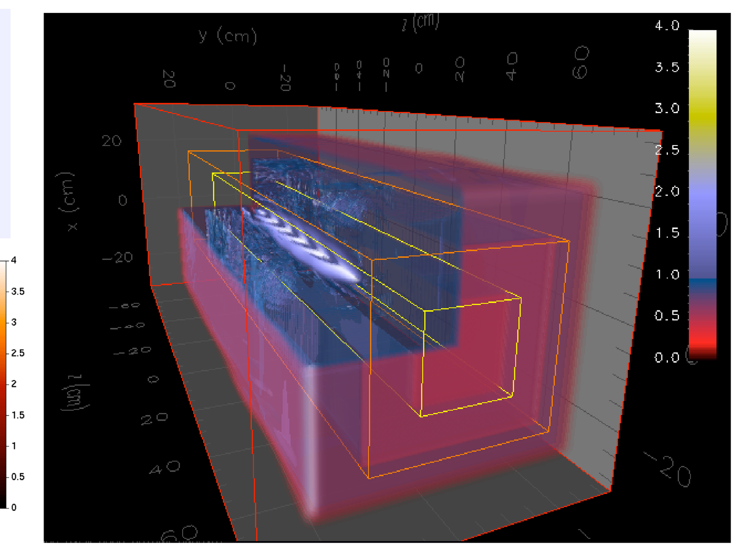

We are exploring the application of AMR to the modeling of laser plasma wakefield accelerators (LWFA). For the simulation of a 10GeV class LWFA stage, the wake wavelength is O[100μm] while the electron bunch and laser wavelength are typically submicron in size. As a result, the resolution required for different parts of the problem may vary by more than two orders of magnitude in each direction.

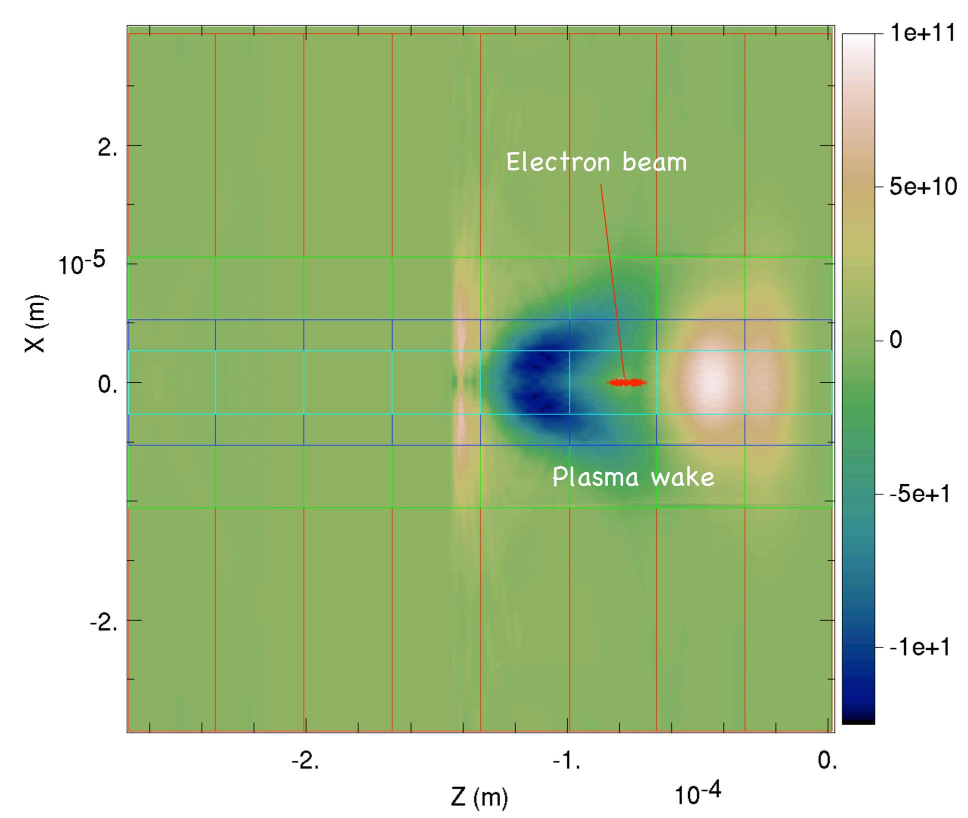

Preliminary results from simulations in a boosted frame (γ=10) of a scaled 10 GeV class stage, varying the transverse resolution with and without mesh refinement patches (using up to 3 levels of mesh refinement), shows that the mesh refinement algorithm implemented in Warp allows relaxation of the resolution of the main grid transversely while preserving the overall accuracy as measured on the evolution of the beam emittance.